Supplement of Atmos. Chem. Phys., 25, 18267–18290, 2025
https://doi.org/10.5194/acp-25-18267-2025-supplement
© Author(s) 2025. CC BY 4.0 License.

Atmospheric Chemistry and Physics
Open Access
EGU

Supplement of

The influence of climate variability on transatlantic flight times

Corwin J. Wright et al.

Correspondence to: Corwin J. Wright (c.wright@bath.ac.uk)

The copyright of individual parts of the supplement might differ from the article licence.

Table S1. Table showing the number of individual flights between each airport-pair, travelling *from* the column airports *to* the row airports.Three-letter codes indicate the airports located as shown in main Figure 2a,b.

	ATL	BOS	BRU	CDG	CLT	CVG	DFW	DTW	DUS	EWR	FRA	IAD	IAH	JFK	MCO	MIA	MSP	MUC	ORD	PHL	RSW	STL	TPA	TXL	VIE	YUL	YYZ
ATL			104	60							1132														42		
BOS			120	55							517							61									
BRU	100	122				146				87				273					68								
CDG	60	56						100		32		109	102	27		49	88		134							92	109
CLT																		17									
CVG			145																								
DFW											83																
DTW				96							241																
DUS										259				155					129								
EWR			84	32					260		273							24									
FRA	1139	522					89	243		288		168	181	543	55	61			197	613	16	17	38			30	559
IAD				104							166													16	136		
IAH				107							180																
JFK			275	22					149		518							160							119		
MCO											54																
MIA				40							50																
MSP				85																							
MUC		61			18					24				162					220							76	
ORD			69	132					128		192							218							104		
PHL											621																
RSW																											
STL											16																
TPA											37																
TXL												17															
VIE	42											137		120					105							43	38
YUL			15	90							27							75							43		
YYZ				105							554														39		

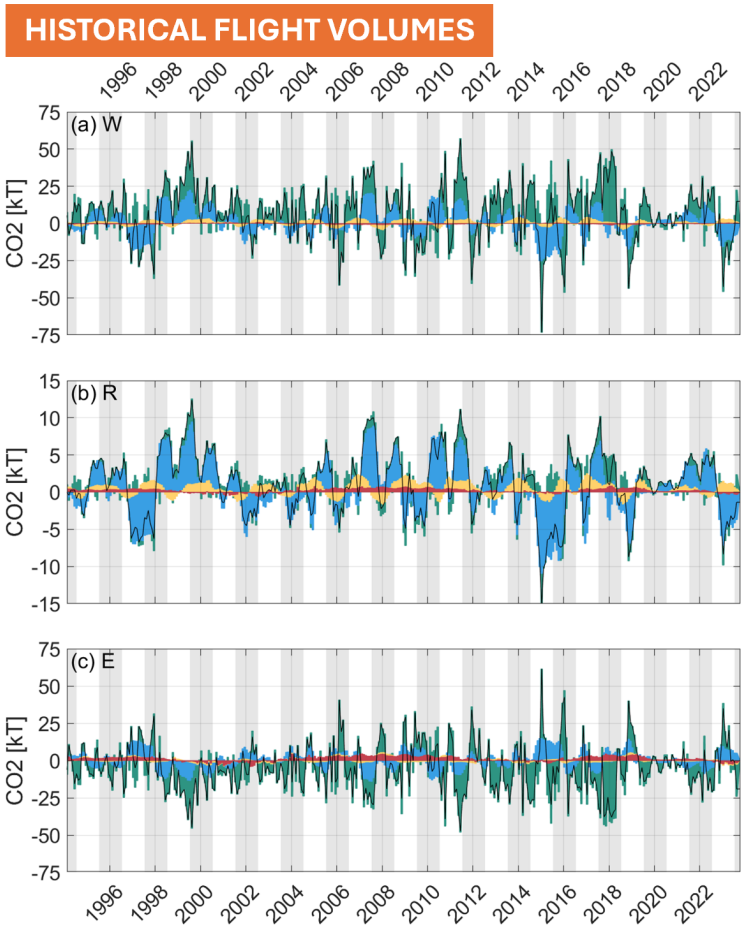

Figure S1. Estimated monthly costs due to climate-index-associated delays from June 1994 to March 2024, in kilotonnes of CO_2 for (a) westwards (b) round-trip (c) eastwards flights at real historical flight volumes. Data are shown as stacked histograms, i.e. the total effect due to a specific index is the difference between that and the next index in the direction of the zero axis. Indices have been ordered for this process such that the slowest-varying (TSI) is closest to the axis and the fastest-varying (NAO) is furthest from the axis. A thin black line shows the net cost summed over all indices for each month.

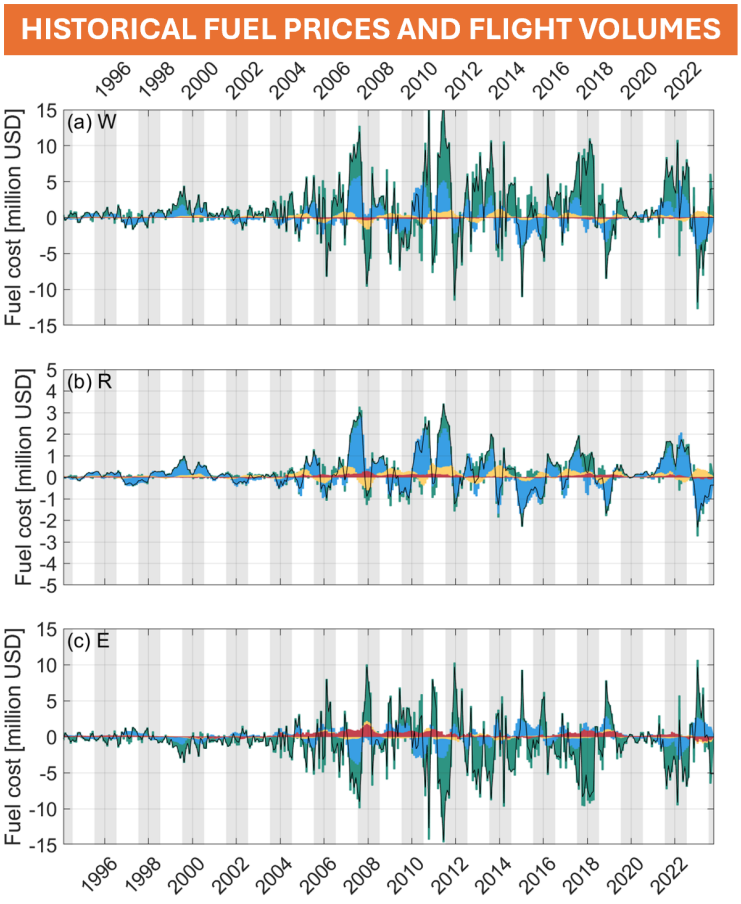

Figure S2. Estimated monthly costs due to climate-index-associated delays from June 1994 to March 2024, in millions of US dollars for (a) westwards (b) round-trip (c) eastwards flights at real historical flight volumes and fuel prices. Data are shown as stacked histograms, i.e. the total effect due to a specific index is the difference between that and the next index in the direction of the zero axis. Indices have been ordered for this process such that the slowest-varying (TSI) is closest to the axis and the fastest-varying (NAO) is furthest from the axis. A thin black line shows the net cost summed over all indices for each month.

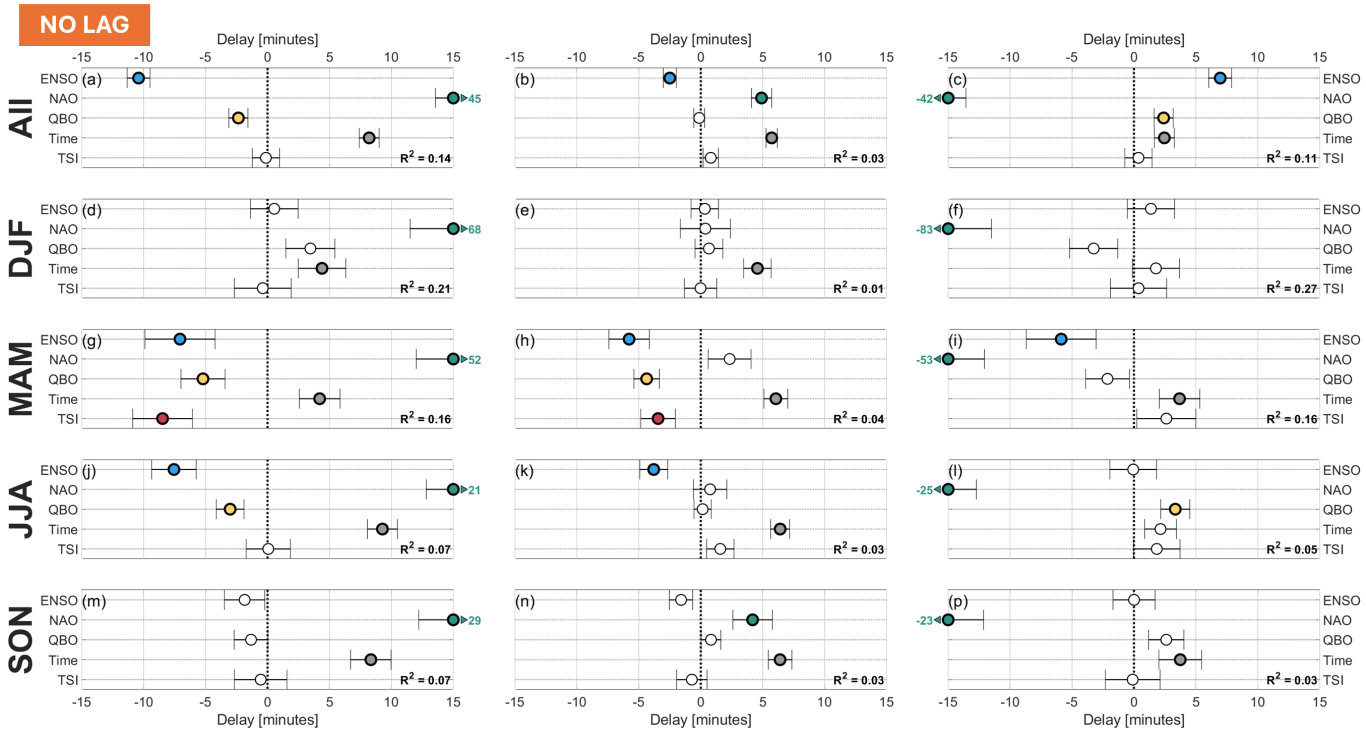

Figure S3. Delay regression coefficients computed over all flights in (a-c) our dataset, (d-f) DJF, (g-i) MAM, (j-l) JJA and (m-p) SON, for flights in the (a,d,g,j,m) westward, (b,e,h,k,n) round-trip and (c,f,i,l,p) eastward direction. Unlike in the main manuscript, no lag has been applied to any dataset. Within each panel, rows shows the regression coefficient estimated over all flights against the climate index marked at the end of the row, with bars to either side of the symbol indicating the uncertainty on that coefficient. Coloured markers with bold outlines indicate estimates significant at the 5% level, and white markers with narrower outlines non-significant estimates. Coefficients are given as delays in minutes on a typical flight duration, with negative values indicating earlier-than-average arrival. The adjusted R^2 of the fit combining all indices is indicated at the bottom right of each panel as text. Horizontal axis ranges have been selected to optimise for visibility of all values, and accordingly some estimates for the NAO fall off the edge of their panel; these are indicated by an arrow and numeric indicator at the end of the relevant row showing the central value, but with the marker and error bars shown as if the estimate was centred at the edge of the panel.

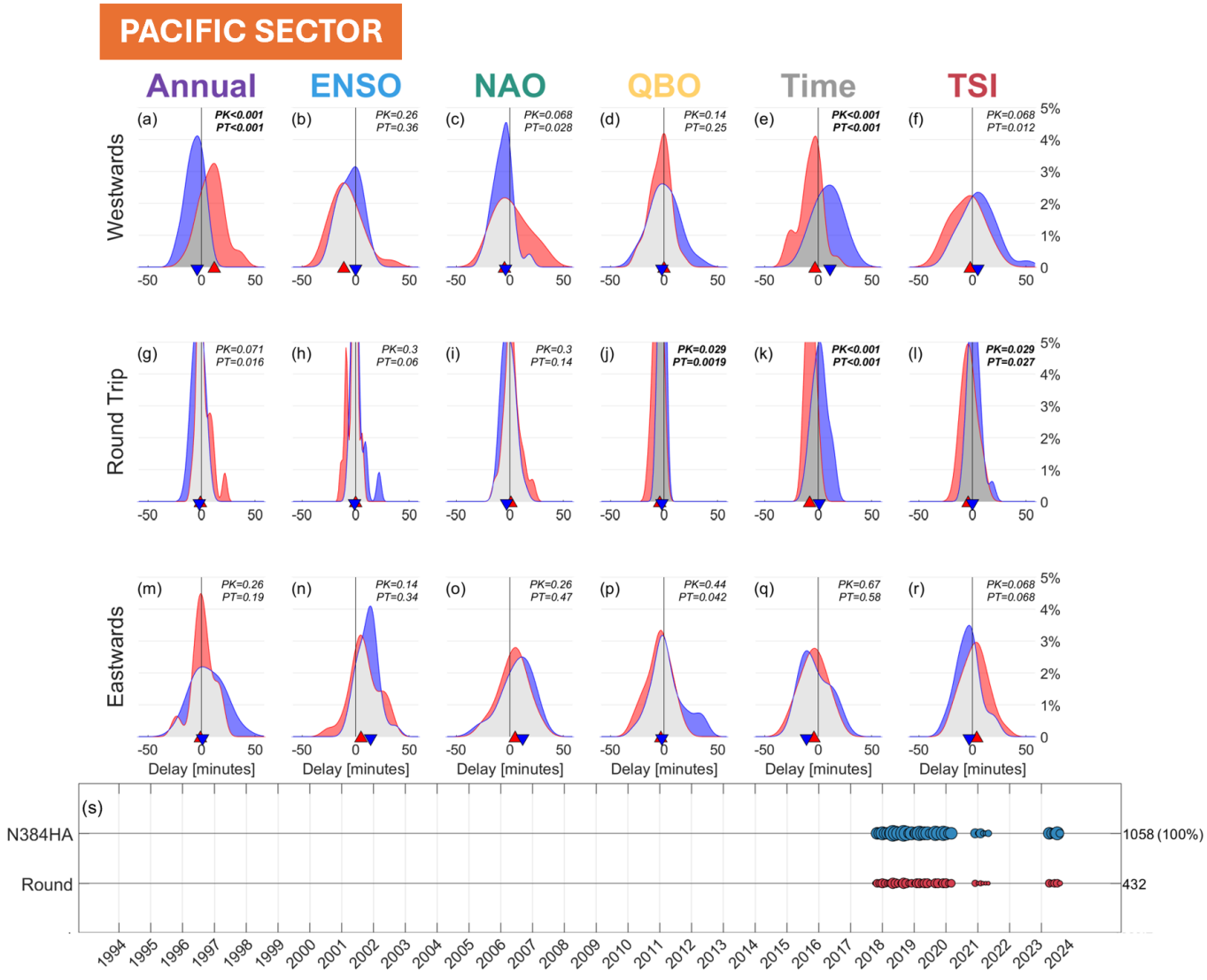

Figure S4. (a-r) Kernel density functions (KDFs) for the top (red) and bottom (blue) 20% of flights by each index between Honolulu and the US West Coast. KDFs are shown for flights in the (a-f) westwards and (m-r) eastwards directions and for (g-l) composite round trips. Columns from left to right show results split on the basis of (a,g,m) Annual, (b,h,n) ENSO, (c,i,o) NAO, (d,j,p) QBO, (e,k,q) Time and (f,l,r) TSI indices. Overlap between the two KDFs are shown in dark grey if the difference between the two KDFs is statistically significant at the 5% level on a two-sample Kolmogorov-Smirnoff test and light grey otherwise, with the numeric K-S test result shown at top right marked as 'PK'. The results of a two-sampled t-test are also shown, marked as 'PT'. Triangle markers on the horizontal axis indicate the median value in each subset of the data, using the same red/blue colour coding. (s) Number of flights per month in the dataset. Each row represents an individual plane, identified by tail number at far left, with bubble sizes showing total flights by that plane each month, summed at right. The bottom dataset, labelled 'round', is the number of round trips each month as defined in the main manuscript.